Int. J. Electrochem. Sci., 14 **(2019)** 4350 – 4360, doi; 10.20964/2019.05.64

International Journal of
ELECTROCHEMICAL
SCIENCE
www.electrochemsci.org

Sea urchin-like Al-doped MnO_2 nanowires with excellent cycling stability for supercapacitor

Yuhan Zeng[1,§], *Yuan Cong*[1,§],*Tongtong Jiang*[1], *Chuanxiang Zhang*[1], *Yaxin Gao*[1], *Hongqi Shi*[2], *Yuming Dai*[1,*]

[1] Jiangsu Key Laboratory of Advanced Structural Materials and Application Technology, School of Materials Engineering, Nanjing Institute of Technology, Nanjing 211167, P.R. China
[2] College of Materials Science and Engineering, Nanjing University of Technology, Nanjing 211816, P.R. China
[*]E-mail: Y.M.Dai@hotmail.com
§ Yuhan Zeng and Yuan Cong contributed equally.

Received: 12 September 2018 / *Accepted:* 3 October 2018 / *Published:* 10 April 2019

Homogenous Al-doped MnO_2 supercapacitor materials with excellent electrochemical properties are synthesized by employing an one-step hydrothermal method in this study. The optimal sample shows morphologies of sea urchin-like micro-spheres, which consists of uniform nanowires with diameters of approximate 30 nm. The Al-doped MnO_2 has enhanced crystallinity and electrical conductivity than the pure MnO_2, which is beneficial to the supercapacitive performance. The optimal Al-doped MnO_2 elctrode material exhibits a high specific capacitance of 101 $F \cdot g^{-1}$ at a high scan rate of 200 $mV \cdot s^{-1}$ and a remarkable long-term cycling stability of 99.6% capacitance retention over 20,000 charge/discharge at 5 $A \cdot g^{-1}$. These results indicate that the sea urchin-like Al-doped MnO_2 nanowires have extensive application prospects in supercapacitors.

Keywords: Al-doped MnO_2, sea urchin-like structure, supercapacitors

1. INTRODUCTION

Recently, supercapacitors have attracted extensive attentions as one of the novel energy storage devices since they show the high power density and long-term cycling stability [1-7]. The electrode materials play a crucial role in the performance and cost of supercapacitors. Among various electrode materials, MnO_2 is widely recognized as a promising candidate because of its high theoretical specific capacitance (SC, 1370 $F \cdot g^{-1}$) and low cost [8-11]. Unfortunately, MnO_2 exhibits the poor native electrical conductivity (EC) and low electroactive area (EA) actually, which are in response to its very small SC values [12-15]. In order to enhance the SC of MnO_2, many studies have been carried out to improve the

EC and/or EA by combining it with conductive materials [16-20]. However, it has been proved that the combinations with other materials will introduce different interfaces, resulting in the deteriorative cycling stability of the electrode materials [21, 22].

To avoid introducing different interfaces, one straightforward strategy is to fabricate homogeneous materials, such as doping [23-26]. Al is an ideal doping element for metal oxides due to its appropriate radius and its structural stability in the materials [27-29]. And hence, a one-step synthesis of Al-doped MnO_2 was developed, in order to obtain the enhanced SC and cycling stability. In this design, a small amount of Al atoms can occupy the tunnels of MnO_2 and substitute the Mn atoms owing to the radius of Al atom is slightly smaller than that of Mn atom, which will increase the bonding energy and reduce the cell volume of the doped MnO_2. Thus, the Al-doped MnO_2 will have a more stable and orderly structure, which is hardly to deform in the cyclic charge/discharge process and shows excellent cycling stability [30].

In this work, the sea urchin-like Al-doped MnO_2 nanowires were synthesized by a facile one-step hydrothermal method. The hierarchical structure provides large EA, high EC as well as high stability. Meanwhile, Al-doping not only generates crystal defects to remarkably enhance the conductivity, but also stabilizes the structure to improve the rate capability. The unique Al-doped morphology contributes to excellent long-term cycling stability of 99.6% capacitance retention over 20,000 charge/discharge cycles at 5 $A\cdot g^{-1}$.

2. EXPERIMENTAL SECTION

2.1 Fabrications

The sea urchin-like Al-doped MnO_2 were fabricated via a one-step hydrothermal method. 4 mmol $KMnO_4$, 0.4 mmol $Al_2(SO_4)_3\cdot 18H_2O$ and 6 mmol $MnSO_4\cdot H_2O$ were dissolved in 40 mL ultrapure water under continuous stirring. The mixed solution was sealed in a Teflon-lined stainless-steel autoclave and hydrothermally treated at 140 °C for 2 hours. Then the obtained specimens were collected by centrifugation and washed by ultrapure water for five times, then dried in a vacuum oven at 50 °C for 12 hours. The pure MnO_2 is prepared by a similar method as described above, except that there is no addition of $Al_2(SO_4)_3\cdot 18H_2O$.

2.2 Structure Characterization

The field emission scanning electron microscopy (SEM, Merlin Compact, Zeiss) equipped with an energy-dispersive spectrometer (EDS, Aztec X-max 50, Oxford), transmission electron microscopy (TEM, JEM-2100, JEOL), X-ray diffraction (XRD, Ultima-IV, Rigaku) and Raman analysis (Invia, Renishaw) with 514 nm wavelength laser were utilized to analyze the morphologies, microstructures, composition of the as-obtained electrodes, respectively.

2.3 Electrochemical Tests

To fabricate the electrode for the electrochemical tests, the as-prepared Al-doping MnO_2 was mixed with 20 wt.% conducting agent (10 wt.% acetylene black and 10 wt.% carbon fiber) and 5 wt.% polytetrafluoroethylene (PTFE) latex as binder. A slurry composed of the above mixtures was subsequently spread on a nickel foam piece with the area of 1 cm^2. And then, the pieces were dried at room temperature for 0.5 h to remove the solvent and finally pressed at 10 MPa to ensure good adherence between the electrode material and nickel foam current collector.

The cyclic voltammetry (CV), galvanostatic charge/discharge measurements (GCD) and electrochemical impedance spectroscopy (EIS) were conducted in 1 M Na_2SO_4 solution at room temperature [31]. An electrochemical workstation (CHI660D, Chenhua) with a three electrode configuration was utilized, where the as-prepared electrode, Ag/AgCl standard electrode and Pt plate acted as the working electrode, reference electrode and the counter electrode, respectively. CV tests were performed over a voltage range of -0.2 to 0.6 V, and the scan rates ranged from 1 to 200 $mV{\cdot}s^{-1}$. GCD measurements were conducted at various current densities from 1 to 20 $A{\cdot}g^{-1}$. Capacitance retention was measured on a battery analyser (C5-100, BettaTeQ). The SC value of the electrodes tested by GCD was evaluated via the following formula.

$$SC = \frac{I\Delta t}{m\Delta V} \tag{1}$$

where I is the applied current (A), Δt is the time of discharge (s), m is the mass of the active materials in the electrodes (g), ΔV is the potential window (V).

3. RESULTS AND DISCUSSION

The SEM image with the low magnification (Figure 1a) indicates that the as-prepared Al-doped MnO_2 shows the sea urchin-like micro-spherical morphology. The high-magnification image (Figure 1b) of a micro-sphere in Figure 1a reveals that it is consist of uniform nanowires with diameters of 30±5 nm. The energy dispersive spectroscopy spectrum (Figure S1, Supplementary material) demonstrates that the Al is doped in the sample with an atomic ratio of 1.20%. Furthermore, the compositional elements of Mn, Al and O are found homogeneously distributed in the structures of the sample, according to the SEM image and the corresponding EDS elemental mapping images (Figure 1c-f).

The TEM image (Figure 2) also indicates that the sample is consist of nanowires. The selected area electron diffraction (SAED) pattern of the nanowires displays the structural characteristics of MnO_2, as presented in the inset in Figure 2. And there is no evidence of Al compounds, which further proves that the Al was successfully doped in the MnO_2.

As shown in Figure 3a, XRD patterns of Al-doped MnO_2 and the pure MnO_2. The diffraction peaks corresponding to the planes of the crystalline structure can be indexed to standard α-MnO_2 (JCPDS No. 44-0141) completely. There are no other compounds' peaks, indicating that the Al-doping does not change the crystal structure of α-MnO_2. And this is consistent with the SEAD result. Moreover, the intensity of diffraction peaks of the Al-doped MnO_2 increased clearly, suggesting a better crystallinity after Al-doping. The Al-doped MnO_2 and the pure MnO_2 were further characterized by Raman spectra (Figure 3b). The band at 645 cm^{-1} represents the symmetric stretching vibration of Mn-O. Furthermore, the higher intensity of the Al-doped MnO_2 also reveals that the crystallinity of the Al-doped MnO_2 is better than the pure MnO_2. That is probably due to the radius of Al atom is slightly smaller than Mn atom, the cell volume shrinks and the structure of the Al-doped MnO_2 will be more stable and orderly when partial Al atoms replace Mn atoms. The structure illustration is shown in Figure 3c.

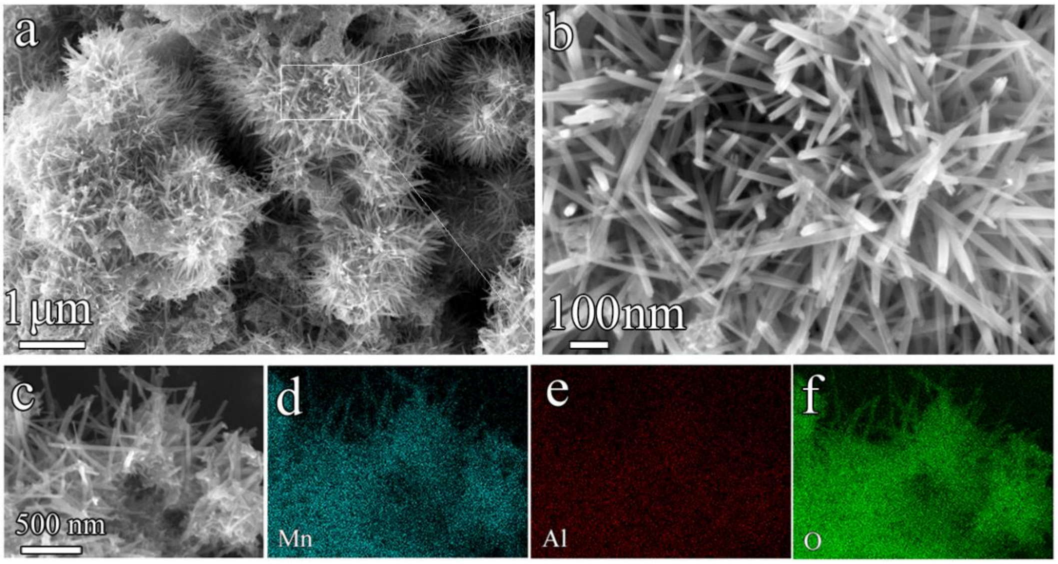

Figure 1. (a, b) SEM images and (c-f) EDS mapping of the optimal Al-doped MnO_2 sample

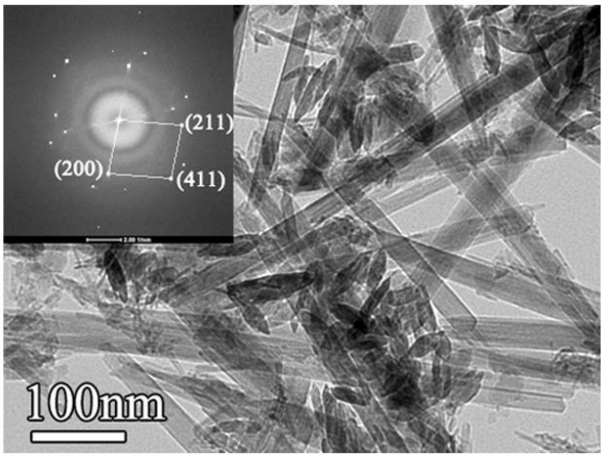

Figure 2. TEM image of the optimal Al-doped MnO_2 sample

Figure 4a represents the CV curves of as-prepared Al-doped MnO_2 at various scan rates from 1 to 200 $mV\cdot s^{-1}$. As the curves exhibited, the shapes are almost rectangular without obvious redox humps, meaning the decent capacitive behavior. It seems to be more appreciate for supercapacitors as referred to the previously reported studies [32-35]. The CV curves change from the standard rectangle shape into the quasi-rectangular shape with the increasing of scan rates, which is might because of the limited diffusion of ions between active material surface and solution. By contrast, the CV curve of the pure MnO_2 at 200 $mV\cdot s^{-1}$ displays a much smaller area obviously (Figure 4b), which indicates that the pure MnO_2 has lower SC than the Al-doped MnO_2. Therefore, it is concluded that the doped Al atoms can play a significant role on enhancing the performance of MnO_2. As testified in similar works [36-38], doping Al can notably improve the conductivity of MnO_2, which is in response to our obtained curves. The calculated SC values of the two samples are plotted in Figure 4c. The SC of the Al-doped MnO_2 at 200 $mV{\cdot}s^{-1}$ is 101 $F{\cdot}g^{-1}$, which is to our knowledge a high value reported for homogeneous manganese oxides at such high scan rate. The SC of the Al-doped MnO_2 decreases gradually with the increasing of scan rates, the value at 200 $mV{\cdot}s^{-1}$ is merely a 31% loss compared with that at 20 $mV{\cdot}s^{-1}$ (147 $F{\cdot}g^{-1}$). However, the SC of the pure MnO_2 at 200 mV s^{-1} reduces to 34 $F{\cdot}g^{-1}$ rapidly, which is 58% decrement of the value at 20 $mV{\cdot}s^{-1}$ (92 $F{\cdot}g^{-1}$). The high rate capability of the Al-doped MnO_2 is mainly contributed by the sea urchin-like nanowires with large electroactive area, which facilitate the adsorption/desorption of ions in the electrolyte. To further characterize the electrochemical properties of the Al-doped MnO_2, the GCD test was measured. The GCD curves (Figure 4d) at current densities of 1 to 20 $A{\cdot}g^{-1}$ exhibit symmetric sloping voltage profiles, which indicates the characteristic of electric double-layer capacitance that is in accordance with the CV results.

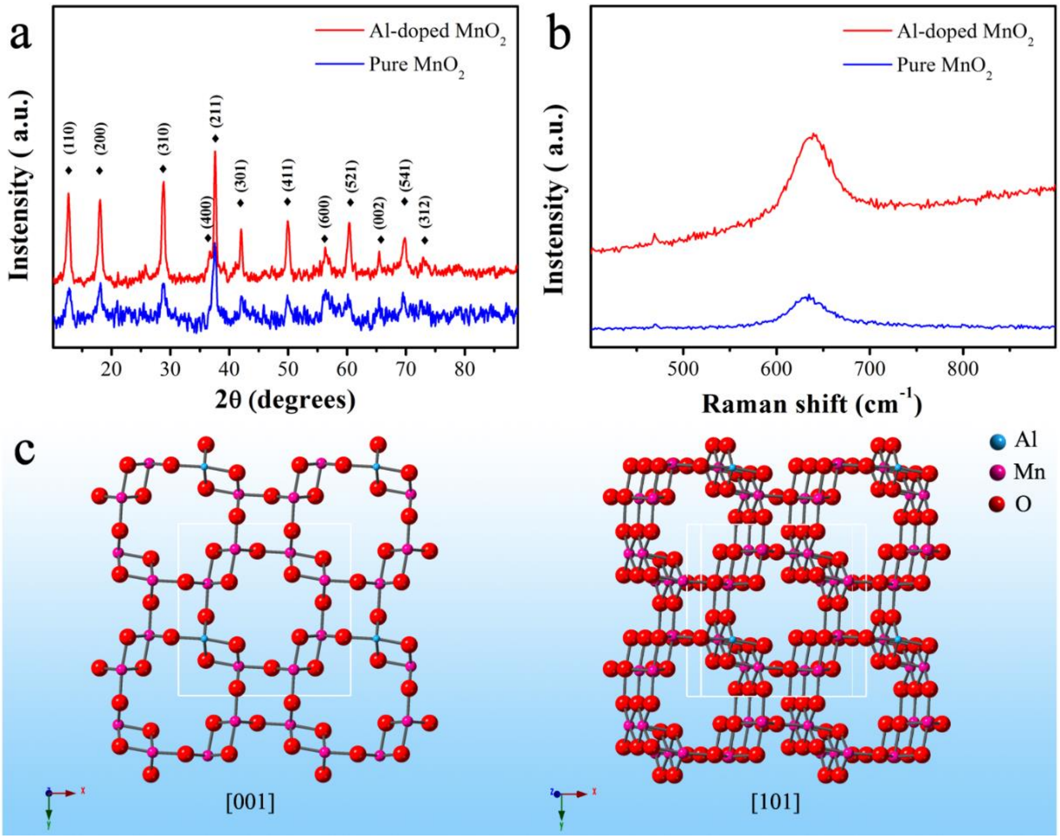

Figure 3. (a) XRD, (b) Raman spectra of the optimal Al-doped MnO_2 and the pure MnO_2 samples and (c) structure models of the Al-doped MnO_2

The EIS analysis were conducted to investigate the EC of the Al-doped MnO_2 and the pure MnO_2. The Nyquist plots of the two samples are shown in Figure 5a. The diameter of semicircle in high frequency region of the Al-doped MnO_2 is smaller than that of the pure MnO_2, which reveals that the Al-doped MnO_2 has a lower charge transfer resistance. The straight line in low frequency region of the

Al-doped MnO_2 has a higher slope, reflecting a lower diffusion resistance and better capacitive behaviour after Al doping.

The cycling stability as one of the most important characteristics for high performance supercapacitor can be shown in Figure 5b. The measurement result indicates that the Al-doped MnO_2 has an excellent long-term cycling stability of 99.6% capacitance retention over 20,000 cycles at 5 $A \cdot g^{-1}$. As far as we know, the value is the highest capacitance retention in the relevant literatures. The capacitance retention of the Al-doped MnO_2 reaches the maximum value (130.1%) after about 4000 cycles. This phenomenon is attributed to the self-activation of the electrode material [39, 40]. However, the pure MnO_2 loses about 60% of their original capacitance at about 500 cycles, and the capacitance retention is only 11.3% over 20,000 charge/discharge cycles. We suppose that the excellent long-term cycling stability of the Al-doped MnO_2 to be due to the cell volume shrink, which is caused by partial Al atoms replace Mn atoms in the cell. Similar doped MnO_2 has been prepared in the reported study and exhibited 91% capacitance retention over 15,000 cycles [38].

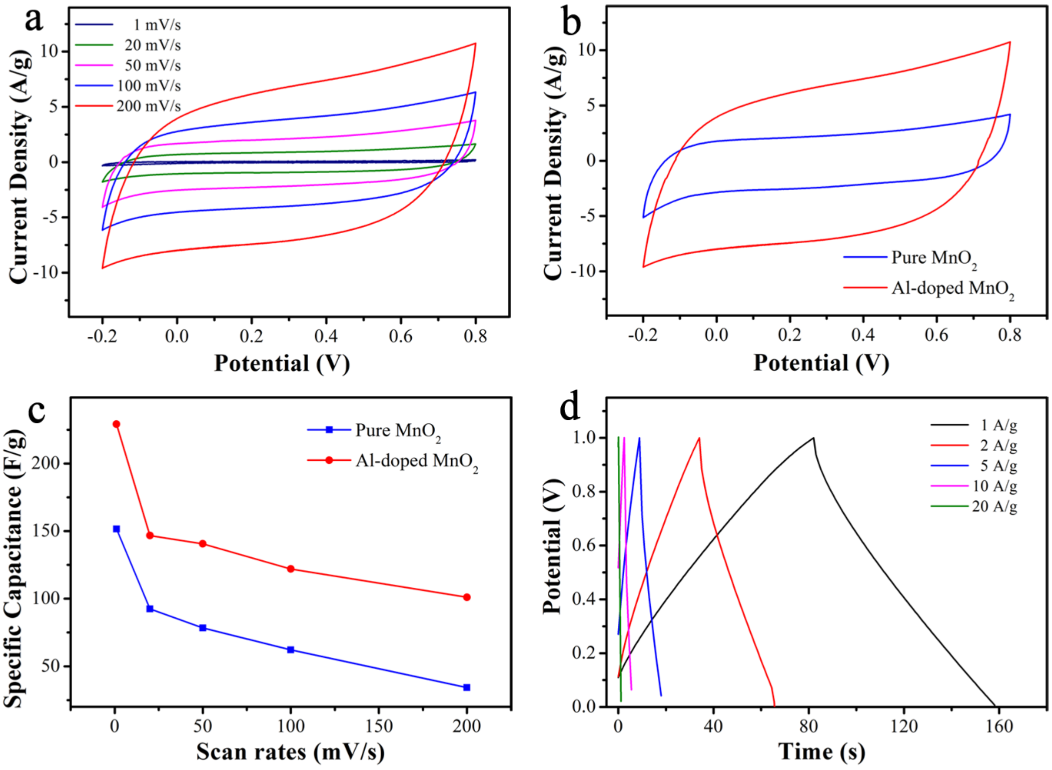

Figure 4. (a) CV curves of the optimal Al-doped MnO_2 sample at various scan rates, (b) CV curves of the optimal Al-doped MnO_2 and the pure MnO_2 samples at 200 $mV \cdot s^{-1}$, (c) calculated SC of the two samples at various scan rates, (d) GCD curves of the Al-doped MnO_2 sample at various current densities

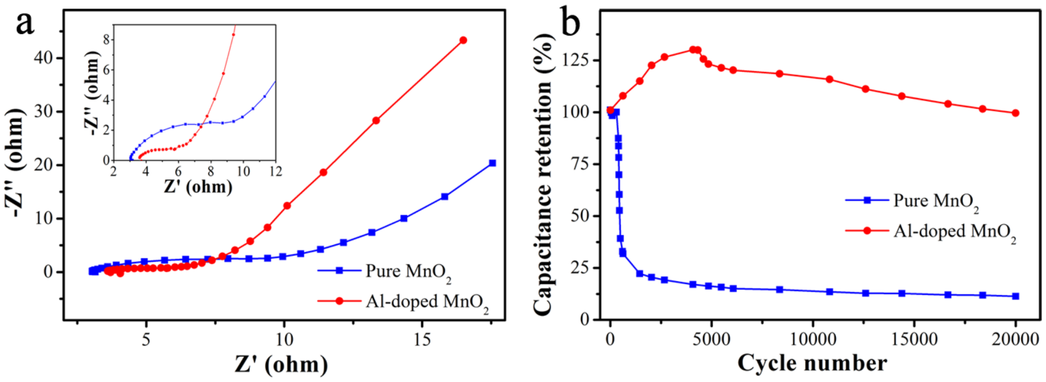

Figure 5. (a) EIS analysis and (b) capacitance retention at 5 A·g^{-1} over 20,000 cycles of the optimal Al-doped MnO_2 and the pure MnO_2 samples

4. CONCLUSIONS

In summary, a one-step hydrothermal method is employed to synthesize sea urchin-like Al-doped MnO_2 nanowires with a superior SC of 101 F·g^{-1} at 200 mV·s^{-1} and an excellent long-term stability of 99.6% capacitance retention over 20,000 cycles at 5 A·g^{-1}. This is owing to the improved structure stability of the cell volume shrink after Al-doping. Thus, the as-prepared Al-doped MnO_2 is the promising candidate to the high performance electrode materials for supercapacitors.

ACKNOWLEDGMENTS

This work was supported by the Outstanding Scientific and Technological Innovation Team in Colleges and Universities of Jiangsu Province, the National Natural Science Foundation of China (51402150), the Scientific Research Foundation of Nanjing Institute of Technology (CKJA201502, JCYJ201606) and the Practice Innovation Program for College Students of Jiangsu Province (201811276).

SUPPLEMENTARY INFORMATION

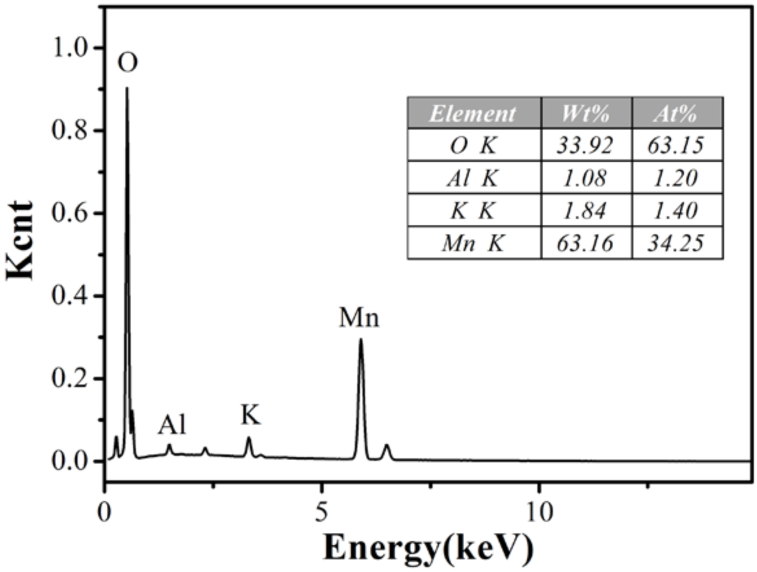

Element	*Wt%*	*At%*
O K	*33.92*	*63.15*
Al K	*1.08*	*1.20*
K K	*1.84*	*1.40*
Mn K	*63.16*	*34.25*

Figure S1. EDS pattern of the optimal Al-doped MnO_2 sample.

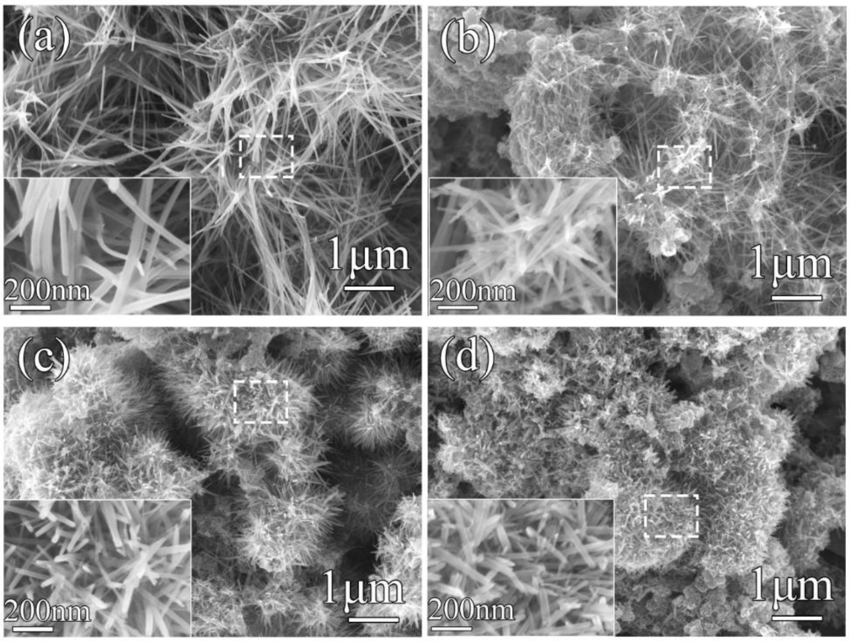

Figure S2. SEM images of the products obtained by using (a) 0 mM, (b) 1 mM, (c) 10 mM and (d) 20 mM $Al_2(SO4)_3 \cdot 18H_2O$ while other conditions are the same as with the synthesis of the optimal Al-doped MnO_2 sample. Insets are further magnifications of the marked rectangles.

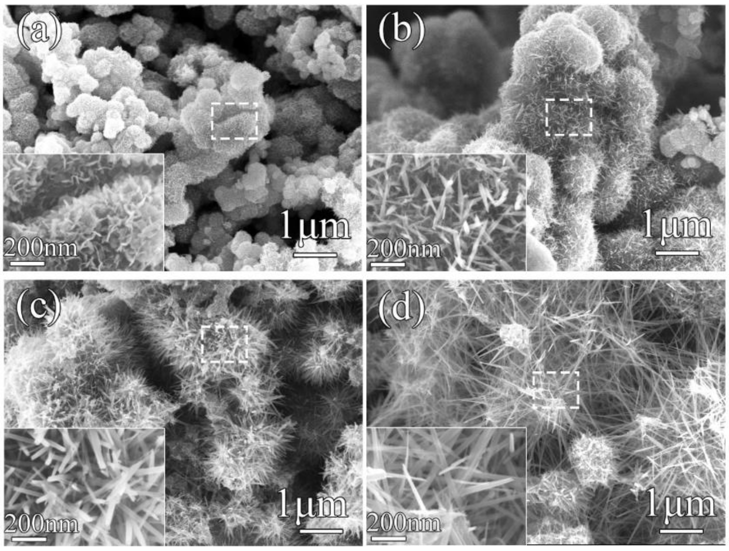

Figure S3. SEM images of the products prepared at (a) 50 °C, (b) 70 °C, (c) 140 °C and (d) 200 °C while other conditions are the same as with the synthesis of the optimal Al-doped MnO_2 sample. Insets are further magnifications of the marked rectangles.

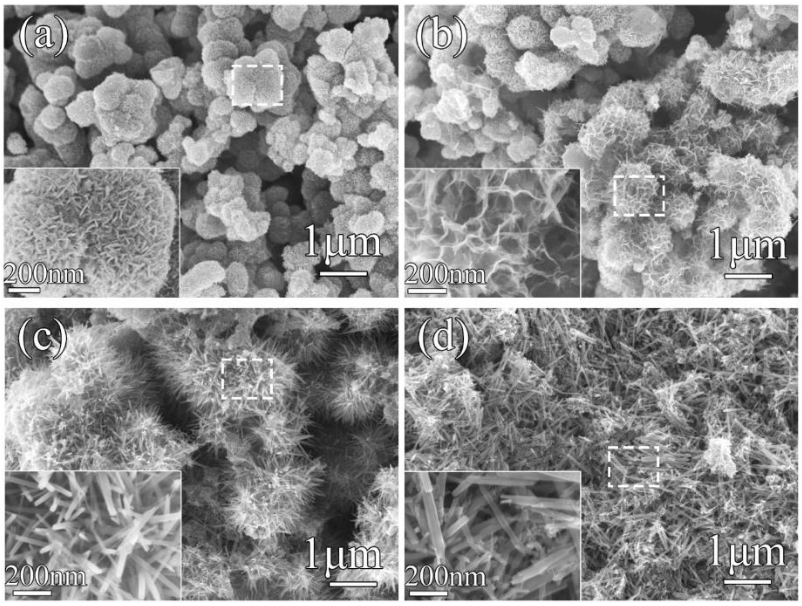

Figure S4. SEM images of the products fabricated for (a) 1 h, (b) 1.5 h, (c) 2 h and (d) 3 h while other conditions are the same as with the synthesis of the optimal Al-doped MnO_2 sample. Insets are further magnifications of the marked rectangles.

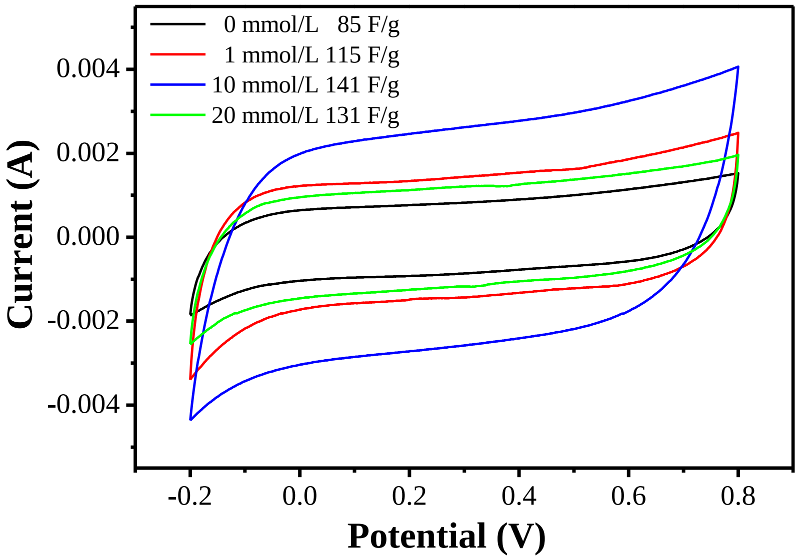

Figure S5. CV curves of the products in Figure S2 at a scan rate of 50 mV/s.

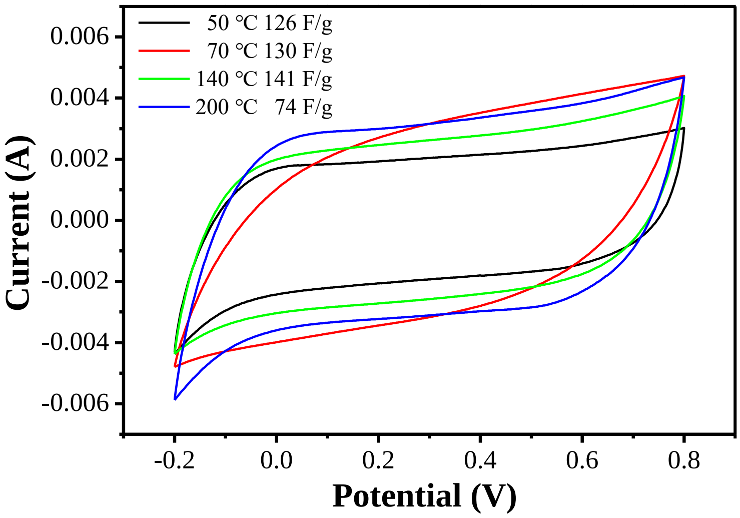

Figure S6. CV curves of the products in Figure S3 at a scan rate of 50 mV/s.

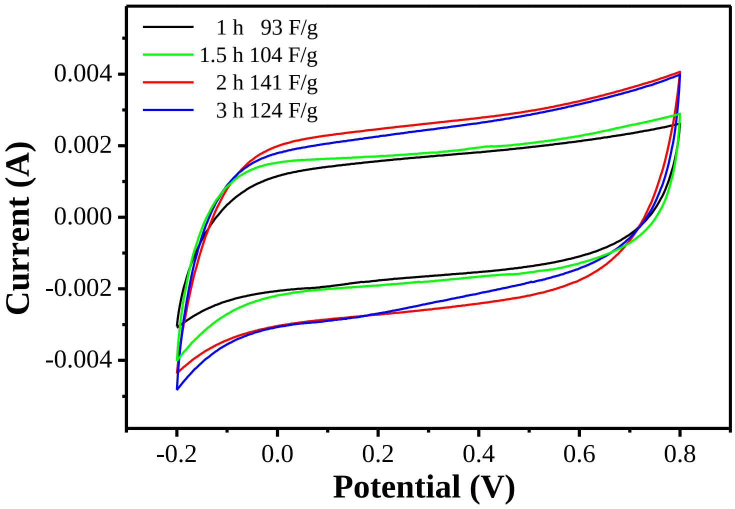

Figure S7. CV curves of the products in Figure S2 at a scan rate of 50 mV/s.

References

1. P. Zhang, F. Zhu, F. Wang, J. Wang, R. Dong, X. Zhuang, O. G. Schmidt and X. Feng, *Adv. Mater.*, 29(2017)1604491.
2. K. Li, T. Zhao, H. Wang, S. Zhang and C. Deng, *J. Mater. Chem. A*, 6(2018)1561.
3. J. Gou, S. Xie, Y. Liu and C. Liu, *Electrochim. Acta*, 210(2016)915.
4. D. V. Lam, K. Jo, C. Kim, J. Kim, H. Lee and S. Lee, *ACS Nano*, 10(2016)11351.
5. J. Zhou, Q. Li, C. Chen, Y. Li, K. Tao and L. Han, *Chem. Eng. J.*, 350(2018)551.
6. P. Gao, P. Metz, T. Hey, Y. Gong, D. Liu, D. D. Edwards, J. Y. Howe, R. Huang and S. T. Misture, *Nat. Commun.*, 8(2017)14559.
7. X. Wang, R. S. Chandrabose, Z. Jian, Z. Xing and X. Ji, *J. Electrochem. Soc.*, 163(2016)A1853.
8. S. Bag and C. R. Raj, *J. Mater. Chem. A*, 4(2016)587.
9. Z. Lv, Y. Luo, Y. Tang, J. Wei, Z. Zhu, X. Zhou, W. Li, Y. Zeng, W. Zhang, Y. Zhang, D. Qi, S. Pan, X. J. Loh and X. Chen, *Adv. Mater.*, 30(2018)1704531.
10. Z. Huang, Y. Song, D. Feng, Z. Sun, X. Sun and X. Liu, *ACS Nano*, 12(2018)3557.
11. Y. Wang, Y. Zhang, D. Dubbink and J. E. Ten Elshof, *Nano Energy*, 49(2018)481.

12. Q. Zhu, K. Liu, J. Zhou, H. Hu, W. Chen and Y. Yu, *Chem. Eng. J.*, 321(2017)554.
13. P. Liu, Y. Zhu, X. Gao, Y. Huang, Y. Wang, S. Qin and Y. Zhang, *Chem. Eng. J.*, 350(2018)79.
14. S. Ortaboy, J. P. Alper, F. Rossi, G. Bertoni, G. Salviati, C. Carraro and R. Maboudian, *Energ. Environ. Sci.*, 10(2017)1505.
15. R. A. Davoglio, G. Cabello, J. F. Marco and S. R. Biaggio, *Electrochim. Acta*, 261(2018)428.
16. S. Kumar, G. Saeed, N. H. Kim and J. H. Lee, *J. Mater. Chem. A*, 6(2018)7182.
17. X. Zheng, Z. Han, W. Yang, F. Qu, B. Liu and X. Wu, *Dalton T.*, 45(2016)16850.
18. C. Hsieh, D. Tzou, W. Lee and J. Hsu, *J. Alloy Compd.*, 660(2016)99.
19. X. Y. Liu, M. Zhou, C. Chen and Y. X. Zhang, *Ceram. Int.*, 43(2017)10595.
20. Q. Lv, S. Wang, H. Sun, J. Luo, J. Xiao, J. Xiao, F. Xiao and S. Wang, *Nano Lett.*, 16(2016)40.
21. X. Fan, Z. Yang and Z. Liu, *Chinese J. Chem.*, 34(2016)107.
22. G. Cheng, C. Si, J. Zhang, Y. Wang, W. Yang, C. Dong and Z. Zhang, *J. Power Sources*, 312(2016)184.
23. O. Lupan, L. Chow, L. K. Ono, B. R. Cuenya, G. Y. Chai, H. Khallaf, S. Park and A. Schulte, *J. Phys. Chem. C*, 114(2010)12401.
24. J. L. Kang, A. Hirata, L. J. Kang, X. M. Zhang, Y. Hou, L. Y. Chen, C. Li, T. Fujita, K. Akagi and M. W. Chen, *Angew. Chem. Int. Edit.*, 52(2013)1664.
25. Y. Gao, J. A. Syed, H. Lu and X. Meng, *Appl. Surf. Sci.*, 360(2016)389.
26. X. Chang, L. Zang, S. Liu, M. Wang, H. Guo, C. Wang and Y. Wang, *J. Mater. Chem. A*, 6(2018)9109.
27. X. Chen, C. Long, C. Lin, T. Wei, J. Yan, L. Jiang and Z. Fan, *Electrochim. Acta*, 137(2014)352.
28. M. Yu, H. Sun, X. Sun, F. Lu, G. Wang, T. Hu, H. Qiu and J. Lian, *Int. J. Electrochem. Sc.*, 8(2013)2313.
29. J. Huang, J. Wei, Y. Xiao, Y. Xu, Y. Xiao, Y. Wang, L. Tan, K. Yuan and Y. Chen, *ACS Nano*, 12(2018)3030.
30. S. Zhang and N. Pan, *Adv. Energy Mater.*, 5(2015)1401401.
31. Y. Dai, S. Tang, S. Vongehr and X. Meng, *ACS Sustain. Chem. Eng.*, 2(2014)692.
32. B. Liu, Y. Liu, H. Chen, M. Yang and H. Li, *J. Power Sources*, 341(2017)309.
33. D. P. Dubal, O. Ayyad, V. Ruiz and P. Gomez-Romero, *Chem. Soc. Rev.*, 44(2015)1777.
34. Y. Wang, J. Zeng, J. Li, X. Cui, A. M. Al-Enizi, L. Zhang and G. Zheng, *J. Mater. Chem. A*, 3(2015)16382.
35. Z. K. Ghouri, M. S. Akhtar, A. Zahoor, N. A. M. Barakat, W. D. Han, M. Park, B. Pant, P. S. Saud, C. H. Lee, H. Y. Kim, *J. Alloy Compd.*, 642(2015)210.
36. Q. Gao, J. X. Wang, B. Ke, J. F. Wang, Y. Q. Li, *Ceram. Int.*, 44(2018)18770.
37. A. V. Radhamani, M. K. Surendra, M. S. R. Rao, *Appl. Surf. Sci.*, 450(2018)209.
38. Z. M. Hu, X. Xiao, C. Chen, T. Q. Li, L. Huang, C. F. Zhang, J. Su, L. Miao, J. J. Jiang, Y. R. Zhang, J. Zhou, *Nano Energ*, 11(2015)226.
39. X. H. Lu, D. Z. Zheng, T. Zhai, Z. Q. Liu, Y. Y. Huang, S. L. Xie and Y. X. Tong, *Energ. Environ. Sci.*, 4(2011)2915.
40. Y. Zhao, M. Lu, P. Tao, Y. Zhang, X. Gong, Z. Yang, G. Zhang and H. Li, *J. Power Sources*, 307(2016)391.